Modeling of transdermal fluorescence measurements from first-in-human clinical trials for renal function determination using fluorescent tracer agent MB-102

Kimberly M. Shultz[a], Martin P. Debreczeny[b], Richard B. Dorshow[b], Jennifer E. Keating[a], and Kate L. Bechtel[a]

[a]Triple Ring Technologies Inc., 39655 Eureka Drive, Newark, CA, USA;
[b]MediBeacon Inc., 1100 Corporate Square Drive, Helix Center, Suite 175, St. Louis, MO, USA

ABSTRACT

The fluorescent tracer agent 3,6-diamino-2,5-bisN-[(1R)-1-carboxy-2-hydroxyethyl]carbamoylpyrazine, designated MB-102, is cleared from the body solely by the kidneys. A prototype noninvasive fluorescence detection device has been developed for monitoring transdermal fluorescence after bolus intravenous injection of MB-102 in order to measure kidney function. A mathematical model of the detected fluorescence signal was created for evaluation of observed variations in agent kinetics across body locations and for analysis of candidate instrument geometries. The model comprises pharmacokinetics of agent distribution within body compartments, local diffusion of the agent within the skin, Monte Carlo photon transport through tissue, and ray tracing of the instrument optics. Data from eight human subjects with normal renal function and a range of skin colors shows good agreement with simulated data. Body site dependence of equilibration kinetics was explored using the model to find the local vasculature-to-interstitial diffusion time constant, blood volume fraction, and interstitial volume fraction. Finally, candidate instrument geometries were evaluated using the model. While an increase in source-detector separation was found to increase sensitivity to tissue optical properties, it reduced the relative intensity of the background signal with minimal effect on the measured equilibration kinetics.

Keywords: Fluorescence, model, Monte Carlo, renal function, pharmacokinetics, transdermal measurement

1. INTRODUCTION

The fluorescent tracer agent 3,6-diamino-2,5-bisN-[(1R)-1-carboxy-2-hydroxyethyl]carbamoylpyrazine, designated MB-102,[1] has been designed to be cleared from the body solely by the kidneys. As it is neither metabolized or cleared from the body by any other mechanism, the change in concentration of MB-102 after a bolus administration can be used to monitor kidney function. The concentration of MB-102 has been demonstrated to be equally effective as Iohexol in determining glomerular filteration rate (GFR).[2,3] The fluorescence of MB-102 can be measured transcutaneously to monitor the changing concentration of the agent.

A transcutaneous fluorescence measurement instrument was built for the first-in-human clinical study of MB-102.[3] In that study, the kinetics of the equilibration of the agent into the measurement region were observed to vary by measurement location on the body. Additionally, signal artifacts were observed due to motion and variations in tissue optical properties. This paper describes a model built to explain the observed clinical measurements and to inform future instrument design.

Further author information: (Send correspondence to K.M.S.)
K.M.S.: E-mail: kshultz@tripleringtech.com,
M.P.D.: E-mail: mdebreczeny@medibeacon.com,
R.B.D.: E-mail: rdorshow@medibeacon.com,
J.E.K.: E-mail: jkeating@tripleringtech.com,
K.L.B.: E-mail: kbechtel@tripleringtech.com

Reporters, Markers, Dyes, Nanoparticles, and Molecular Probes for Biomedical Applications IX
edited by Samuel Achilefu, Ramesh Raghavachari, Proc. of SPIE Vol. 10079, 100790I
 · doi: 10.1117/12.2251068

2. METHODS

A model was built to explain the data gathered from the transcutaneous fluorescence measurement instrument. The model was implemented in MATLAB (Mathworks, Natick, MA) and CUDA (NVIDIA, Santa Clara, CA). It comprised three components: a ray tracing optical model of the instrument (MATLAB); a Monte Carlo optical model of photon transport through tissue including fluorescence (CUDA and MATLAB); and a pharmacokinetic model of fluorescent agent distribution (MATLAB).

Ray tracing was used to model the instrument optics including the fiber bundle, turning prism, and adhesives. Additionally, a theoretical instrument with discrete source and detector locations immediately adjacent to the skin surface was modeled. The instrument was treated as being in perfect optical contact with the skin, without an intervening air gap.

MCA, a custom GPU accelerated optical Monte Carlo simulator developed by Triple Ring Technologies (Newark, CA), was used to model the light transport from instrument exit, through the tissue or phantom, to instrument reentry. MCA follows the algorithm of Fang's MCX[4] for photon transport and adds capabilities for modeling both distributed and local fluorescence. MCA has been validated against MCX for diffuse reflectance measurements as well as against both *in vivo* and *in vitro* experimental measurements for diffuse reflectance and fluorescence.

A multi-layer skin model was built including depth-varying concentration of the fluorescent agent. The model comprises 20 µm thick layers, each of which can have different optical properties including concentrations of fluorescent agent.

The skin model was derived from skin models and measurements in the literature[5–12] and has been validated *in vivo* using spatially resolved diffuse reflectance measurements. The model uses distinct scattering parameters for each major skin layer (epidermis, dermis, and subcutaneous). The scattering values (Table 1) were selected based on Ref. 10 and 5, scaled by by 70% to match typical values observed in the human population observed in other studies by the authors. The major skin layers were further subdivided into sublayers (Fig. 1). The absorption was varied based on the chromophores composition of individual skin sublayers, based on an average blood volume fraction of 1% (Table 2). The absorption of blood was calculated using the data of Ref. 13 by assuming a hemoglobin concentration of 150 g/L with an average oxygen saturation of 60%.[9] Interstitial fluid was treated as water using the absorption data from Ref. 14. Lipids used the data from Ref. 15. The absorption of melanin was modeled using Eqn. 1[16] for the absorption of a melanosome. A melanosome volume fraction of 4% was modeled, corresponding roughly to Fitzpatrick[17] skin type 3 (see Eqn. 2).

$$6.6 \cdot 10^{11} \cdot \lambda^{-3.33} \mathrm{cm}^{-1} \tag{1}$$

Each sublayer also has a unique index of refraction and anisotropy.[18]

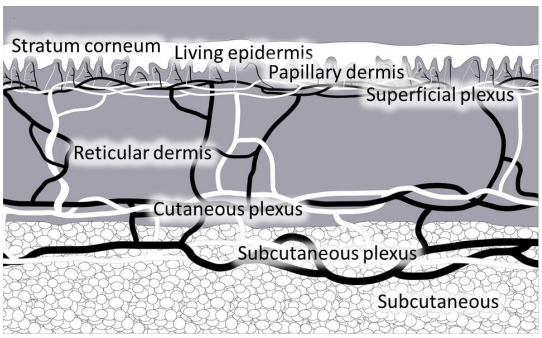

Figure 1: Skin model sublayers.

The excitation light was simulated as a monochromatic source at 455 nm. The emission light was simulated at 10 distinct wavelengths from 525 nm to 615 nm, with the results weighted by the emission spectrum of the fluorescent agent.

Table 1: Reduced scattering coefficients for each major skin layer. The nominal values were used for all simulations except for the explorations of optical property variations. Values listed are for the excitation light (455 nm) and emission light (560 nm), respectively.

Layer	Low value	Nominal value	High value	Literature
Epidermis	$40\,cm^{-1}$, $28\,cm^{-1}$	$56\,cm^{-1}$, $39\,cm^{-1}$	$72\,cm^{-1}$, $50\,cm^{-1}$	$80\,cm^{-1}$, $56\,cm^{-1}$([10])
Dermis	$27\,cm^{-1}$, $18\,cm^{-1}$	$38\,cm^{-1}$, $25\,cm^{-1}$	$49\,cm^{-1}$, $32\,cm^{-1}$	$55\,cm^{-1}$, $35\,cm^{-1}$([10])
Epidermis	$8.3\,cm^{-1}$, $7.1\,cm^{-1}$	$12\,cm^{-1}$, $10\,cm^{-1}$	$15\,cm^{-1}$, $13\,cm^{-1}$	$17\,cm^{-1}$, $14\,cm^{-1}$([5])

Table 2: Volume fraction of chromophores (excluding MB-102), anisotropy, and index of refraction in each skin sublayer.

Layer	Blood	Melanosomes	Water	Lipids	Anisotropy	Index of Refraction
Stratum Corneum	0%	0%	5%	0%	0.86	1.5
Living Epidermis	0%	4%	20%	0%	0.8	1.34
Papillary Dermis	1.1%	0%	20%	22%	0.9	1.4
Superficial Plexus	1.1%	0%	20%	22%	0.95	1.39
Reticular Dermis	.83%	0%	20%	22%	0.8	1.4
Cutaneous Plexus	4.1%	0%	20%	22%	0.95	1.38
Subcutaneous Pexus	4.1%	0%	9%	90%	0.75	1.44
Subcutaneous	0.8%	0%	9%	90%	0.75	1.44

To investigate the effect of optical property variations (both inter- and intra-subject), the nominal values of chromophore concentrations and scattering were adjusted. The nominal blood volume was halved and doubled. The oxygen saturation of the blood was increased to 80% and decreased to 30%. The scattering was increased and decreased by about 30%, and the higher scattering values from the literature were used as well. Finally, the volume fraction of melanin in the epidermis was varied based on Eqn. 2, derived from the ranges in Ref. 19.

$$f_{mel} = 0.5\% \cdot 2^{\text{Fitzpatrick skin type}} \tag{2}$$

Clinical measurements were taken at four different body sites: the forehead, the sternum, the medial upper arm, and the lateral lower ribcage (denoted trunk). Each location was simulated. The primary difference in skin from different body locations studied in the literature is the thickness of the epidermis and dermis.[20] The subcutaneous thickness varies as well, but is at least a few millimeters thick in all locations. As the light does not penetrate past a few millimeters, those variations were not included in the model. The thicknesses of each skin layer at each body site are displayed in Table 3. The modeled thickness of the living epidermis and reticular dermis were adjusted to account for these variations. There are also expected to be differences in vascularization but that information is not readily available for the body sites under investigation so it was not included in the model.

The concentration of the fluorescent agent was allowed to vary with depth based on the pharmacokinetics of distribution in the vasculature and skin. The optical contribution of the agent was assumed to only occur in the vasculature and interstitial fluid. The concentration in the vasculature was assumed uniform throughout the body, modeled by a typical pharmacokinetic equation with a double exponential decay representing diffusion into the central compartment (the alpha stage) and clearance by the kidneys, parameterized by time constants τ_{renal} and τ_{alpha}, respectively (Eqn. 3). The alpha component was weighted by the fractional contribution of that term (F_{alpha}) which was allowed to vary freely when matching the model to clinical measurements.

$$C_{vasculature} = C_{vasculature,initial}\left(e^{-t/\tau_{renal}} + F_{alpha}e^{-t/\tau_{alpha}}\right) \tag{3}$$

Table 3: Thickness of skin layers for each modeled body site.

	Thickness			
Layer	Forehead	Sternum	Arm	Trunk
Epidermis	100 µm	80 µm	80 µm	80 µm
Dermis	0.78 mm	1 mm	1.34 mm	1.34 mm

Table 4: Modeled blood vesel diameter by skin layer.

Papillary Dermis (Capillaries) (Forehead; Sternum; Arm/Trunk)	Dermis	Cutanous/Subcutaneous Plexi, Subcutaneous
3 µm; 5 µm; 7 µm	11 µm	25 µm

It was assumed that the diffusion of the agent from the blood into the interstitial space did not have a significant effect on the concentration of the agent in the vasculature except as captured by the alpha term.

The concentration of MB-102 in the interstitial fluid was modeled with a differential equation representing diffusion between the vasculature and the interstitial space and vertical diffusion within the interstitial space (Eqn 4). Each type of diffusion was characterized by a separate diffusion coefficient: D_{vi} representing vasculature-to-interstitial-space diffusion, and D_z representing vertical diffusion within the interstitial space.

$$\frac{\partial C_{vasculature}}{\partial t} = D_{vi}\left(C_{vasculature} - C_{interstitial}\right) + D_z \frac{\partial C_{interstitial}}{\partial z} \tag{4}$$

The vasculature-to-interstitial-space diffusion coefficient was scaled in each layer proportional to the total vessel surface area. The surface area for each layer was calculated from the blood volume and the average vessel diameter[21,22] (Table 4), with decreased vessel diameters in the cappilary layer based on typical sun exposure of the body sites.[23] The total agent concentration in each layer was computed by weighting the concentrations of agent within the vasculature and interstitial fluid by the local partial volumes of interstitial fluid and blood.

The model parameters were adjusted to match the data from the clinical study. The adjusted parameters were the local blood volume fraction, the local interstitial fluid volume fraction, and the vasculature-to-interstitial diffusion coefficient. The intra-interstitial fluid diffusion coefficient was explored but did not have a significant effect on the results within the plausible range of values. For each subject, the plasma measurements were used to derive the agent concentration within the blood. A universal scaling factor to translate the measured plasma concentrations to blood concentrations was derived by finding the best fit across all subjects. The plasma data had insufficient sampling density for a subject-specific fit during the alpha stage of the pharmacokinetics, where the agent diffuses into the central compartment. Therefore, an approximate universal alpha-stage coefficient was derived using data from all subjects.

3. RESULTS

3.1 Modeling of clinical study measurements

An example of clinical measurements of MB-102 for a single subject is shown in Fig. 2a. Initially, the different body locations were modeled using only the differences in skin thickness and capillary diameter. Those differences did not have sufficient effect on the modeled kinetics to account for the variations between body sites.

The parameter that best explained the observed variations was the vasculature-interstitial space diffusion coefficient, τ_{vi}. By adjusting τ_{vi}, good agreement was achieved between the clinical measurements and the modeled measurements (Fig. 2b). It is likely that the variations in the diffusion coefficient were caused by variations in the local microvasculature in the skin. Future work will involve analysis of skin biopsies to correlate microvasculature characteristics to the observed diffusion coefficients.

Across the 8 clinical subjects, the forehead and sternum consistently exhibited the fastest equilibration between the vasculature and interstitital space. The arm and trunk locations were slower and more widely varied. A summary of the observed diffusion coeffients is shown in Fig. 3.

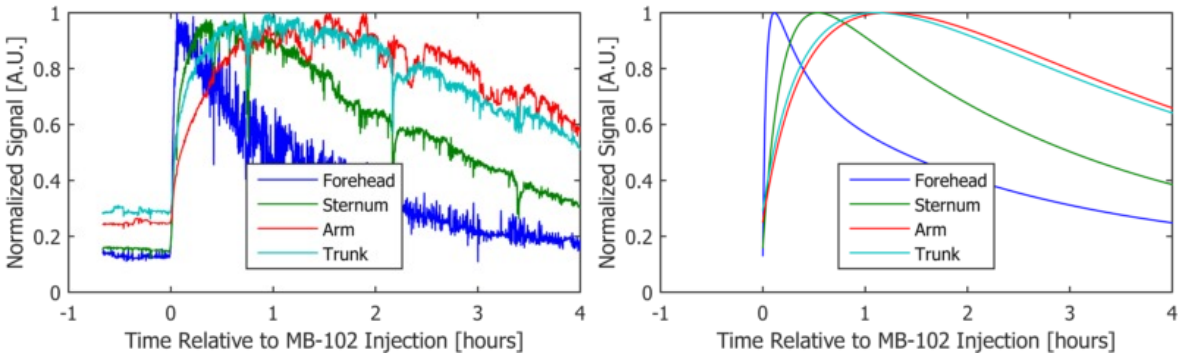

(a) Clinical measurements (b) Modeled measurements

Figure 2: Clinical measurements and measurements simulated by the model. The clinical measurements show the initial background signal due to tissue autofluorescence, the injection and equilibration of the agent, and the renal clearance. There is noise and artifacts in the clinical measurements due to autoregulatory processes changing blood volume and motion artifacts. The background signal from tissue autoofluorescence was included as a constant additive signal in the model. The model shows good agreement with the kinetics observed in the clinical measurements. The faster equilibration kinetics of the forehead and sternum are due to a shorter vasculature-to-interstitial-space diffusion time constant.

Table 5: Vasculature-to-interstitial-space diffusion coefficients (τ_{vi}) modeled in Fig. 2.

	Forehead	Sternum	Arm	Trunk
τ_{vi} [hours]	0.12	0.81	2.2	1.9

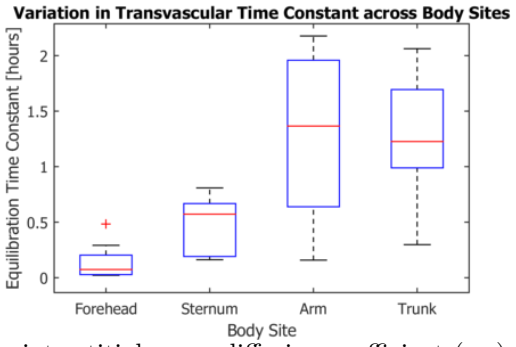

Figure 3: Vasculature-to-interstitial-space diffusion coefficient (τ_{vi}) across 8 clinical subjets.

The modeled concentration of MB-102 in the tissue varied with depth and time (Fig. 4). MB-102 was most concentrated in the regions with dense blood nets at the intersections of the epidermis, dermis, and subcutaneous layers. The diffusion from the vasculature to the local interstitial space was the dominant determinant of the concentration. Vertical diffusion of the agent within the interstitial space only provided a small contribution. The relative concentration of MB-102 by depth only exhibited a small variation with time. This suggests that increasing the effective measurement depth by increasing the separation between the source and detector would not have a large effect on the kinetics (see Section 3.2).

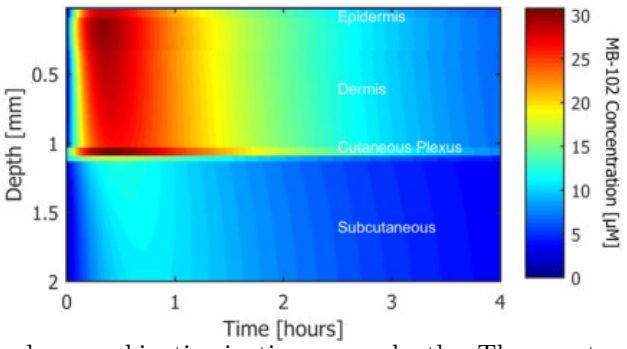

Figure 4: Modeled MB-102 pharmacokinetics in tissue vs. depth. The agent was most concentrated in the regions of higher blood vessel density. The concentration was limited in the subcutaneous due to the smaller interstitial space.

3.2 Effect of optical geometry

The instrument used in the clinical study has overlapping illumination (source) and collection (detector) regions, for a small effective source-detector separation. The effective source-detector separation is the average separation between each possible source location and each possible detection location, weighted by the signal level at each source-detector separation. Due to the extended nature of the source and detection regions of the clinical instrument, the effective source-detector separation was approximately 400 µm. Increasing the separation between the source and detector increases the effective measurement depth. A general rule of thumb for visible light is that the average measurement depth is between a quarter and a half of the source-detector separation, with shallower measurements at shorter wavelengths.

A future instrument could be designed to have discrete illumination and collection regions with a larger effective source-detector separation. To see if this would prove advantageous, simulations were performed for source-detector separations ranging from 0 mm to 5 mm. As the source and detector move farther apart, less light reaches the detector due to absorption and diffusion through scattering. The reflected source light shows a steeper decline with increasing separation as compared to the fluorescent light (Fig. 5). This was caused by the higher absorption and scattering at the source wavelength as compared to the emission wavelength. Thus at longer source-detector separations, the requirements for filtering the reflected source light signal are diminished. An instrument with an effectve source-detector separation of 4 mm would have almost two orders of magnitude less reflected source light relative to the fluorescence intensity as compared to the clinical instrument. Thus an increased source-detector separation would decrease the background signal level that is not due to agent fluorescence.

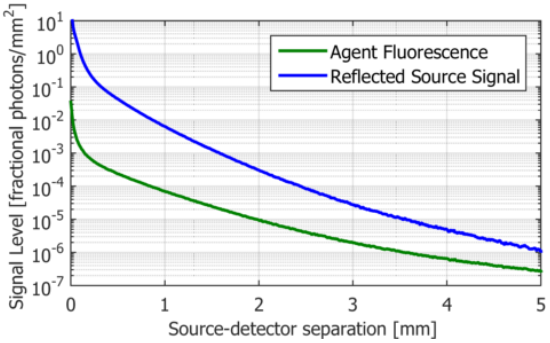

Figure 5: Reflected excitation light and agent fluorescence both decrease with increasing source-detector separation, but the reflected source light diminishes more quickly than the agent fluorescence.

As expected from the limited depth-dependence of the agent pharmacokinetics (seen in Fig. 4), the modeled

fluorescence measurement kinetics are quite similar across source-detector separations, with a small increase in the time to equilibration as the source-detector separation increases (Fig. 6). The impact of instrument design on the rate of equilibration was insignificant in comparison to the effect of the measurement location on the body.

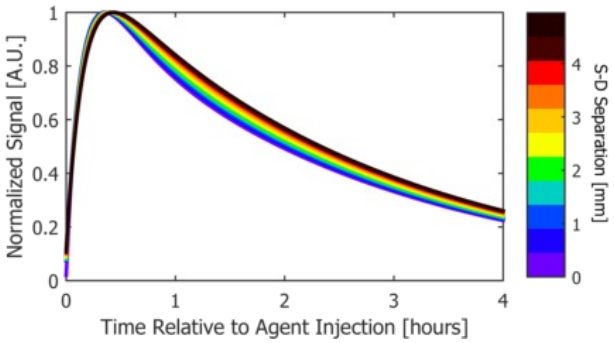

Figure 6: Modeled fluorescence measurement kinetics for varied distances between the source optics and the detection optics. The kinetics exhibit only a small dependence on source-detector separation.

3.3 Effect of optical property variation

There are two cases of optical property variations that must be considered: inter- and intra-subject variations. Inter-subject variations are dominated by the absorption of melanin, and are relevant to determine the dynamic range requirements for the instrument design. Intra-subject measurements do not experience variations in melanin, assuming the measurement is taken in a single location. However, variations in blood volume and oxygenation as well as scattering changes can occur on the same time scale as the renal clearance of MB-102, potentially confounding the measurement.

Fig. 7 shows the effect of melanin concentrations covering the range of the human population. The signal range due to melanin concentration for the clinical instrument was between one and two orders of magnitude. The dynamic range increases slightly with source-detector separation up to approximately 0.5 mm (Fig. 7a). Beyond that distance, the impact of melanin was independent of source-detector separation. This effect was due to the localization of melanin in the epidermis. At shorter source-detector separations, some light was detected that has not fully traversed the epidermis, reducing the effect of melanin concetration. For longer source-detector separations, almost all of the detected light spends the majority of its path in the dermis and subcutaneous where the absorption was lower, passing the epidermis upon entry and exit of the skin only. The vast majority of the fluorescent signal was created below the epidermis, suggesting that the kinetics of the measurement should be unaffected by the concentration of melanin. This was confirmed by the model (Fig. 7b).

Within a single subject, the optical properties of the skin are likely to change over a measurement duration spanning multiple hours. In particular, the blood volume in the skin will vary due to autoregulatory processes. Changes to scattering, generally caused by variations in hydration, and blood oxygen saturation also affect the tissue optical properties. As these can vary during a measurement, they are of concern for measurement accuracy as well as dynamic range requirements. Fig. 8 shows the impact of these variations. At short source-detector separations such as those used in the clinical instrument, the expected intra-subject signal range was approximately a factor of two. The signal range increases along with source-detector separation, reaching over an order of magnitude by 4 mm. While a longer source-detector separation is more sensitive to optical property variations, even the existing clinical instrument is sufficiently sensitive to optical property variations to require an algorithmic correction for those variations.

The model assumes that all changes to blood volume are uniformly distributed throughout the skin. In reality, many of the autoregulatory processes that affect skin blood volume will predominantly affect the capillary layer. This will lead to signal changes more like those due to melanin, as the optical property changes are confined to the top layers of skin. These changes will be more independent of source-detector separation.

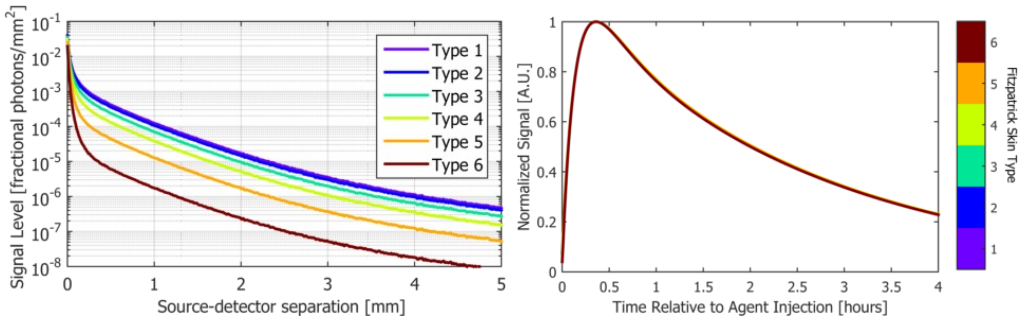

(a) Signal Variations due to Fitzpatrick skin type, shown vs. source-detector separation.

(b) Kinetics of agent signal, normalized to peak signal. The concentration of melanin has no effect on the kinetics.

Figure 7: The influence of skin type (melanin concentration) on the modeled measurements.

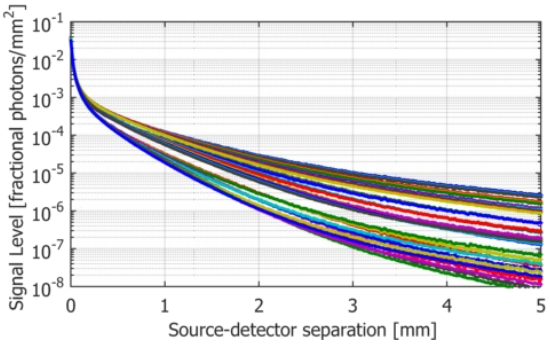

Figure 8: Modeled fluorescence measurement variations at a single point in time across a range of possible intrasubject optical properties (blood volume, blood oxygen saturation, and scattering), shown vs. source-detector separation.

4. DISCUSSION

Having an *in silico* model improves understanding of the interactions of the measurement instrument and physiology. To use a fluorescent agent for transdermal measurements of kidney function, the primary concerns are the measurement kinetics, sensitivity to variations in optical properties, and the size of the background signal. The required complexity and cost of the instrument also must be considered.

The time constants associated with the equilibration kinetics observed in the clinical study at the arm and trunk locations are of similar duration as the time constants associated with renal clearance in healthy subjects. This confounds the calculation of the renal clearance rate. It is desirable to accelerate the kinetics of the measurement through instrument design; unfortunately, the model shows that the optical geometry has only a minimal effect on the observed equilibration time. The underlying cause of the variation in equilibration kinetics is likely due to local variations in microvasculature. To maintain or improve the performance observed at the forehead and sternum sites, it is recommended to investigate regions of the body where the skin is highly perfused.

To calculate the time constant associated with renal clearance, the background signal, due to tissue autofluorescence and reflected excitation light, must be removed. This signal contribution can be measured before injection of the agent, but like the agent signal, it will vary with optical property changes. Therefore, minimizing the background signal will reduce error in the the estimation of the renal clearance time constant. This argues for a longer source-detector separation in a future instrument design. The contribution of reflected excitation light to the measurement can be diminished by using high-rejection interference filters, but this requires quality collimation optics that increase the size and cost of the instrument.

The cost of going to a longer source-detector separation is an increased sensitivity to optical property variations. These variations can be corrected by adding diffuse reflectance measurements and using intrinsic fluorescence algorithmic techniques.[24] Further exploration of the differing effects of optical property variations based on the homogeneity of the effect is warranted: much of the blood volume variation due to autoregulatory processes will be confined to the capillary layer near the surface of the skin.

ACKNOWLEDGMENTS

This work was funded by MediBeacon Inc.

REFERENCES

1. J. E. Bugaj and R. B. Dorshow, "Pre-clinical toxicity evaluation of MB-102, a novel fluorescent tracer agent for real-time measurement of glomerular filtration rate," *Regulatory toxicology and pharmacology: RTP* **72**, pp. 26–38, June 2015.
2. R. B. Dorshow, M. P. Debreczeny, J. C. Fink, and T. C. Dowling, "Initial Clinical Trial Results of a Real-Time Point-of-Care Glomerular Filtration Rate Measurement Utilizing a Novel Fluorescent Tracer Agent," *J Am Soc Nephrol* **26**, p. 259A, 2015.
3. M. P. Debreczeny and R. B. Dorshow, "Development and clinical trial results of a prototype device for trans-cutaneous monitoring of kidney function," in *Proc. of SPIE*, **In Press**, 2017.
4. Q. Fang and D. A. Boas, "Monte Carlo simulation of photon migration in 3{D} turbid media accelerated by graphics processing units," *Optics express* **17**(22), pp. 20178–20190, 2009.
5. A. N. Bashkatov, E. A. Genina, V. I. Kochubey, and V. V. Tuchin, "Optical properties of human skin, subcutaneous and mucous tissues in the wavelength range from 400 to 2000 nm," *Journal of Physics D: Applied Physics* **38**, pp. 2543–2555, Aug. 2005.
6. J. Reuss, "Multilayer Modeling of Reflectance Pulse Oximetry," *IEEE Transactions on Biomedical Engineering* **52**, pp. 153–159, Feb. 2005.
7. I. V. Meglinski and S. J. Matcher, "Computer simulation of the skin reflectance spectra," *Computer Methods and Programs in Biomedicine* **70**, pp. 179–186, Feb. 2003.
8. T. Gambichler, R. Matip, G. Moussa, P. Altmeyer, and K. Hoffmann, "In vivo data of epidermal thickness evaluated by optical coherence tomography: Effects of age, gender, skin type, and anatomic site," *Journal of Dermatological Science* **44**(3), pp. 145–152, 2006.
9. S. L. Jacques, "Optical properties of biological tissues: a review," *Physics in Medicine and Biology* **58**, pp. 5007–5008, July 2013.
10. E. Salomatina, B. Jiang, J. Novak, and A. N. Yaroslavsky, "Optical properties of normal and cancerous human skin in the visible and near-infrared spectral range," *Journal of Biomedical Optics* **11**(6), p. 064026, 2006.
11. D. Yudovsky and L. Pilon, "Retrieving skin properties from in vivo spectral reflectance measurements," *Journal of Biophotonics* **4**, pp. 305–314, May 2011.
12. W. G. Zijlstra, A. Buursma, and W. P. M.-v. d. Roest, "Absorption spectra of human fetal and adult oxyhemoglobin, de-oxyhemoglobin, carboxyhemoglobin, and methemoglobin.," *Clinical Chemistry* **37**, pp. 1633–1638, Sept. 1991.
13. Zijlstra, Buursma, and v. Assendelft, *Visible and Near Infrared Absorption Spectra of Human and Animal Haemoglobin determination and application*, CRC Press, Utrecht; Boston, 1 edition ed., Mar. 2000.
14. S. J. Matcher, M. Cope, and D. T. Delpy, "Use of the water absorption spectrum to quantify tissue chromophore concentration changes in near-infrared spectroscopy," *Physics in Medicine and Biology* **39**, pp. 177–196, Jan. 1994.
15. R. L. van Veen, H. Sterenborg, A. Pifferi, A. Torricelli, and R. Cubeddu, "Determination of VIS-NIR absorption coefficients of mammalian fat, with time-and spatially resolved diffuse reflectance and transmission spectroscopy," in *OSA Biomedical Topical Meeting*, p. SF4, Optical Society of America, 2004.
16. S. L. Jacques, "Skin Optics," *http://omlc.org/news/jan98/skinoptics.html* (Accessed Dec 29 2016), 1998.

17. T. B. Fitzpatrick, "The validity and practicality of sun-reactive skin types I through VI," *Archives of dermatology* **124**(6), pp. 869–871, 1988.
18. I. V. Meglinski and S. J. Matcher, "Quantitative assessment of skin layers absorption and skin reflectance spectra simulation in the visible and near-infrared spectral regions," *Physiological measurement* **23**(4), p. 741, 2002.
19. S. L. Jacques, "Optical Absorption of Melanin," *http://omlc.org/spectra/melanin/* (Accessed 29 Dec 2016).
20. Y. Lee and K. Hwang, "Skin thickness of Korean adults," *Surgical and Radiologic Anatomy* **24**, pp. 183–189, Jan. 2002.
21. I. M. Braverman, "Ultrastructure and Organization of the Cutaneous Microvasculature in Normal and Pathologic States," *Journal of Investigative Dermatology* **93**, pp. 2S–9S, Aug. 1989.
22. I. M. Braverman, "The cutaneous microcirculation," *The Journal of Investigative Dermatology* **5**(1), pp. 3–9, 2000.
23. M. Huzaira, F. Rius, M. Rajadhyaksha, R. R. Anderson, and S. Gonzlez, "Topographic variations in normal skin, as viewed by in vivo reflectance confocal microscopy," *The Journal of Investigative Dermatology* **116**, pp. 846–852, June 2001.
24. R. S. Bradley and M. S. Thorniley, "A review of attenuation correction techniques for tissue fluorescence," *Journal of The Royal Society Interface* **3**, pp. 1–13, Feb. 2006.